Accepted Manuscript

Insights into methane dynamics from analysis of authigenic carbonates and chemosynthetic mussels at newly-discovered Atlantic Margin seeps

N.G. Prouty, D. Sahy, C.D. Ruppel, E.B. Roark, D. Condon et al.

Please cite this article in press as: Prouty, N.G., et al. Insights into methane dynamics from analysis of authigenic carbonates and chemosynthetic mussels at newly-discovered Atlantic Margin seeps. *Earth Planet. Sci. Lett.* (2016), http://dx.doi.org/10.1016/j.epsl.2016.05.023

This is a PDF file of an unedited manuscript that has been accepted for publication. As a service to our customers we are providing this early version of the manuscript. The manuscript will undergo copyediting, typesetting, and review of the resulting proof before it is published in its final form. Please note that during the production process errors may be discovered which could affect the content, and all legal disclaimers that apply to the journal pertain.

Highlights

- Microbial source to USAM methane venting.
- Occurrence of MDACs at ~15 ka and 3 ka along the USAM.
- Link between Pleistocene sediment delivery and occurrence of USAM MDACs.
- Sedimentary framework as predictor of widespread venting along USAM passive margin.

1 **Insights into methane dynamics from analysis of authigenic carbonates and chemosynthetic**
2 **mussels at newly-discovered Atlantic Margin seeps**

3 Prouty[1]*, N.G., Sahy[2], D., Ruppel[3], C.D., Roark[4], E.B., Condon[2], D., Brooke[5], S., Ross[6], S.W.
4 Demopoulos[7], A.W.J.

5 [1]US Geological Survey, Pacific Coastal and Marine Science Center, 400 Natural Bridges Drive Santa Cruz, CA
6 95060 nprouty@usgs.gov
7 [2]Department of Geography, Texas A&M University, College Station, TX 77843
8 [3] NERC Isotope Geosciences Laboratory, British Geological Survey, Nicker Hill, Keyworth NG12 5GG
9 UK
10 [4] US Geological Survey, Woods Hole Coastal and Marine Science Center, Woods Hole, MA 02543
11 [5]Florida State University, Coastal and Marine Laboratory, 3618 Coastal Highway 98 St. Teresa, FL 32358
12 [6]University of North Carolina-Wilmington, Center for Marine Science, 5600 Marvin Moss Ln, Wilmington, NC
13   28409
14 [7]US Geological Survey, Wetland and Aquatic Research Center, 7920 NW 71st St., Gainesville, FL 32653
15 *corresponding author*
16

17 **Abstract**

18 The recent discovery of active methane venting along the US northern and mid-Atlantic margin
19 represents a new source of global methane not previously accounted for in carbon budgets from
20 this region. However, uncertainty remains as to the origin and history of methane seepage along
21 the tectonically inactive passive margin. Here we present the first isotopic analyses of authigenic
22 carbonates and methanotrophic deep-sea mussels, *Bathymodiolus* sp.*,* and the first direct
23 constraints on the timing of past methane emission, based on samples collected at the upper slope
24 Baltimore Canyon (~385 m water depth) and deepwater Norfolk (~1600 m) seep fields within
25 the area of newly-discovered venting. The authigenic carbonates at both sites were dominated by
26 aragonite, with an average $\delta^{13}C$ signature of -47‰, a value consistent with microbially driven
27 anaerobic oxidation of methane-rich fluids occurring at or near the sediment-water interface.
28 Authigenic carbonate U and Sr isotope data further support the inference of carbonate
29 precipitation from seawater-derived fluids rather than from formation fluids from deep aquifers.
30 Carbonate stable and radiocarbon ($\delta^{13}C$ and $\Delta^{14}C$) isotope values from living *Bathymodiolus* sp.
31 specimens are lighter than those of seawater dissolved inorganic carbon, highlighting the
32 influence of fossil carbon from methane on carbonate precipitation. U-Th dates on authigenic
33 carbonates suggest seepage at Baltimore Canyon between 14.7±0.6 ka to 15.7±1.6 ka, and at the
34 Norfolk seep field between 1.0±0.7 ka to 3.3±1.3 ka, providing constraint of the longevity of
35 methane efflux at these sites. The age of the brecciated authigenic carbonates and the occurrence
36 of pockmarks at the Baltimore Canyon upper slope could suggest a link between sediment
37 delivery during Pleistocene sea-level lowstand, accumulation of pore fluid overpressure from
38 sediment compaction, and release of overpressure through subsequent venting. Calculations
39 show that the Baltimore Canyon site probably has not been within the gas hydrate stability zone
40 (GHSZ) in the past 20 ka, meaning that in-situ release of methane from dissociating gas hydrate
41 cannot be sustaining the seep. We cannot rule out updip migration of dissociating methane
42 hydrate that occurs farther down the slope as a source of the venting at Baltimore Canyon, but
43 consider that the history of rapid sediment accumulation and overpressure may play a more
44 important role in methane emissions at this site.

45 Key words: authigenic carbonate; cold seep; AOM; chemosynthesis; mid-Atlantic margin;
46 isotope geochemistry

1. Introduction

48 The distribution of newly discovered seafloor methane seeps along the US Atlantic margin

49 (USAM) (Skarke et al., 2014) has important implications for ocean carbon dynamics (Boetius

50 and Wenzhöfer 2013), continental slope stability and related hazards (Dugan and Flemings 2000;

51 ten Brink et al. 2014), and also the geographic extent of chemosynthetic communities (Quattrini

52 et al. 2015). Whereas seafloor methane venting typically occurs in major hydrocarbon basins

53 such as the Gulf of Mexico or on active margins such as Cascadia, the northern USAM passive

54 margin had long been considered relatively inactive (Skarke et al., 2014). Methane seeps have

55 been documented on the southern USAM, at Cape Fear (L. Brothers et al. 2013) and Blake Ridge

56 (Paull et al. 1995; Van Dover et al. 2003), where they occur at a depth range of 2155 to 2600 m

57 above rising salt diapirs that perturb that gas hydrate stability field (Hornbach et al., 2005), but

58 no such features were known on the northern part of the margin. This assessment was revised

59 when geophysical surveys conducted between 2011 and 2013 identified ~570 gas plumes at

60 water depths of 50-1700 m between Cape Hatteras and Georges Bank (Skarke et al. 2014).

61 Observations at a few of the sites from remotely operated vehicles (ROV) included bubble

62 streams, bacterial mats, chemosynthetic communities, authigenic carbonates, deep-sea corals,

63 and gas hydrate (Skarke et al., 2014; Quattrini et al. 2015). Average contemporary methane

64 emissions from seeps along the entire northern USAM are estimated at ~15 to 90 Mg yr^{-1}

65 (equivalent to 0.95 to 5.66 x 10^6 mol yr^{-1}) based on analysis of ROV bubble observations (Skarke

66 et al. 2014), versus 2.15 to 8.65 x 10^6 mol yr^{-1} in a seep field of Hudson Canyon based on the

67 water column methane concentrations (Weinstein et al., 2016).

68

69   The origin and characteristics of the methane seeps north of Cape Hatteras remain elusive. No

70   underlying salt diapirs have been documented in the seeping areas, and Skarke et al. (2014)

71   postulate that dissociation of gas hydrate and possibly submarine groundwater discharge may

72   play a role in feeding seeps between the outer continental shelf and uppermost continental slope,

73   while the deeper seeps represent leakage of methane through fractured Eocene rocks.

74   Distinguishing among these and other processes that may be responsible for the methane

75   emissions requires direct study of seep fluids, rocks, and organisms. To acquire samples for such

76   studies, the Bureau of Ocean Energy Management (BOEM), the U.S. Geological Survey

77   (USGS), the National Oceanic and Atmospheric Administration (NOAA), and their academic

78   partners initiated a 5-year multi-disciplinary "Atlantic Deepwater Canyons" study focusing on

79   ecologically significant habitats (canyons, cold seeps, hard-bottoms and shipwrecks) in Norfolk

80   Canyon (off Virginia) and overlooking Baltimore Canyon (off Maryland) (Fig. 1). Of the two

81   sites, Baltimore Canyon had been previously investigated in the early 1980s with photographs of

82   a dense community of mussels at ~400 m obtained using a towed camera sled (B. Hecker, pers.

83   comm.), but no further work was conducted in the area until recently. During the Atlantic

84   Deepwater Canyons cruises, we used ROVs designed to support physical and biological

85   sampling to confirm the location of a shallow (~400 m) seep site overlooking Baltimore Canyon

86   in 2012 and, following the discovery of deep-sea gas plumes (NOAA, 2012), identified a new

87   chemosynthetic community at ~1600 m water depth south of Norfolk Canyon in 2013.

88

89   Authigenic carbonates are common at cold seeps and record a robust fingerprint of hydrocarbon

90   seep activity, including local and regional controls on the source and flux of carbon, the

91   conditions under which carbonates formed, and information regarding fluid-sediment and rock

92   interactions (see reviews in Campbell et al., 2006; Suess 2014). Additionally, authigenic

93   carbonates are amenable to uranium (U)-series dating techniques, and can provide key

94   information on the timing and duration of fluid venting at each seep (Teichert et al. 2003; Bayon

95   et al. 2009; Liebetrau et al., 2014). The isotopic composition of shells from chemosynthetic

96   bivalves living close to fluid vents represents an important archive of the nature and variability

97   of the venting. While previous studies have investigated authigenic carbonate formation and cold

98   seeps in other settings (Han et al., 2014; Suess 2014; Bayon et al., 2015) and fluid flow in

99   passive margins (Berndt 2005), this is the first study to examine the origin of the authigenic

100   carbonates, the source fluids, and the timing of methane emissions on the northern USAM. This

101   paper explores the geochemistry, mineralogy, and petrology of authigenic carbonates and bivalve

102   shells recovered by ROVs from both the Norfolk and the Baltimore Canyon seep fields with the

103   aim of tracing the origin and flow pathways of gas and fluids at both sites. Taken together, the

104   geochemical information derived from both authigenic carbonates and bivalve shells collected

105   from seeps in the Baltimore and Norfolk canyons expands our understanding of the origin and

106   occurrence of widespread methane seepage along the US Mid-Atlantic margin

107

108   **2. Methods**

109   2.1 Study site

110   A shallow (~385 m; Fig 2) seep site seaward and south of the location where Baltimore Canyon

111   (38° 03.086 N, 73° 49.379 W) crosses the shelf-break was surveyed and sampled during a 2012

112   cruise (17 Aug–14 Sep) aboard the NOAA ship *Nancy Foster* using the *Kraken II* ROV

113   (University of Connecticut). This site was sampled again in 2013, along with the deeper (1455-

114   1610 m; Fig. 3) Norfolk seep site (36° 51.921 N, 74° 29.574 W) during a cruise (2–18 May)

115   onboard the NOAA ship *Ronald H. Brown* using the *Jason II* ROV (Woods Hole Oceanographic

116   Institution). At the Norfolk seep site, gas bubbles can be traced at least ~600 m above the

117   seafloor (Fig. 3C), as confirmed by USGS surveys on the *R/V Endeavor* in April 2015 (Ruppel et

118   al., 2015a). At the Baltimore Canyon seep field, water column imaging carried out by the USGS

119   in April and September 2015 (Ruppel et al., 2015b) showed that venting is more widespread and

120   diffuse (Fig. 2D). Dense colonies of chemosynthetic mussels, active gas bubbling, and extensive

121   bacterial mats were observed at both seep sites (Fig. 2C and 3D) during the 2012 and 2013 ROV

122   dives. Clams, common at the Blake Ridge seep site (Van Dover et al. 2003), were notably

123   absent, as were tubeworms, a finding that is consistent with a recent survey of chemosynthetic

124   communities from seep sites along the northeastern US continental margin (Quattrini et al.,

125   2015). Seep communities at the Norfolk and Baltimore Canyon seep fields were dominated by

126   the deep-sea mussels of the genus *Bathymodiolus*, which depends on chemosynthetic

127   endosymbiotic bacteria to oxidize sulfur and/or methane for nutrition (Duperron et al. 2011).

128

129   2.2 X-Ray diffraction and petrography

130   Sample mineralogy was determined microscopically in thin sections, and by X-ray diffraction

131   (XRD) using a Philips XRD with graphite monochromator at 40 kV and 45 mA. Step scans were

132   run from 5° to 65° 2θ with 0.02° steps, using CuKα radiation and a count time of 2 s per step.

133   XRD digital scan data were analyzed using the Philips X'Pert High Score search-and-match

134   function to identify minerals. Mineral percentages were determined by multiplying unique peak

135   intensities for each mineral in a sample by relative intensity factors. The products for all

136   minerals in each sample were then summed to 100%. Carbonate content, reported as weight

137 percent (wt%), was determined using a coulometer at the USGS Pacific Coastal and Marine

138 Science Center, Santa Cruz, CA.

139

140 2.3 Stable isotopes

141 Stable carbon ($\delta^{13}C$) and oxygen ($\delta^{18}O$) isotopes were analyzed at the Stable Isotope

142 Geosciences Facility at Texas A&M University. Authigenic carbonate samples were subsampled

143 to isolate the cement and groundmass components. For the mussel shells, carbonate and

144 periostracum (organic rich outer layer) were collected along transects from the umbo to the

145 ventral margin of an individual specimen at discrete distances. Prior to analysis, the

146 periostracum material was acidified to remove inorganic carbon. Data were generated from a

147 Thermo-Finnigan MAT 253 with a Kiel IV Automated Carbonate Prep Device and are reported

148 in per mil (‰) relative to the international reference Pee Dee Belemnite (PDB). Analytical

149 uncertainties (2σ) of 0.04‰ for $\delta^{13}C$ and 0.06‰ for $\delta^{18}O$ are reported based on the long term

150 daily measurements of the international carbonate standard, NBS-19. Seawater samples were

151 measured for $\delta^{18}O$ using a Picarro L2120i cavity ringdown spectrometer at the Stable Isotope

152 Geoscience Facility at Texas A&M University, College Station. Isotope values were calibrated

153 to the VSMOW reference standard using internal reference standards JGULF and KONA. The

154 $\delta^{18}O$ value in VSMOW2 for JGULF is 1.22‰, and for Kona is -6.86‰. Average internal $\delta^{18}O$

155 precision is 0.12 ‰, and an external precision replicate of the same sample is 0.26‰.

156

157 Sulfur isotopes ($\delta^{34}S$) were determined at the Washington State University Stable Isotope Core

158 Laboratory. Mussel gill and seep sediment were combusted with an elemental analyzer (ECS

159 4010, Costech Analytical) coupled to a Delta PlusXP Thermo-Finnigan continuous flow isotope

160   ratio mass spectrometer. Sulfur isotope ratios ($\delta^{34}S$) are reported in per mil (‰) relative to

161   VCDT (Vienna Canyon Diablo Troilite). Analytical accuracy (1σ) of $\delta^{34}S$ was determined by

162   replicate analysis of internal lab standard referenced to IAEA standards, reported as 0.26‰

163   (n=36), bovine internal standard at 0.47‰ (n=18) and sample replicates 0.13‰ (n=9).

164

165   2.4 Strontium isotopes

166   The strontium isotope ($^{87}Sr/^{86}Sr$) compositions of the authigenic carbonates, mussel shells, and

167   seawater samples were determined at the USGS facility at Menlo Park, California. Bottom water

168   samples were filtered using a 0.45 μm glass fiber filter. Authigenic carbonate samples were

169   subsampled to isolate the cement and groundmass components, and mussel shell material was

170   homogenized using an agate mortar and pestle. The mussel shell and authigenic components

171   were leached to remove labile Sr and digested in sealed Teflon vessels. Sr was separated from

172   other ions using a Bio-Rad® AG-502-X8 cation exchange resin with HCl as the eluent. Purified

173   Sr was converted to nitrate form, taken up in 30 μL of 0.15 M H_3PO_4 and loaded onto a Ta

174   ribbon for mass spectrometric measurement. The isotopic composition was measured on a

175   Finnigan MAT 261 multi-collector mass spectrometer using a static collection mode. All

176   reported values of $^{87}Sr/^{86}Sr$ have been corrected for analytical fractionation to the standard

177    $^{88}Sr/^{86}Sr$ ratio of 8.37521, and measurements are precise to ±0.00002 at the 95% confidence

178   level.

179

180   2.5 Radiocarbon (^{14}C) analysis

181   Radiocarbon (^{14}C) analysis was performed on subsamples of authigenic carbonates and mussel

182   shells collected from dead and live mussel specimens. Samples were prepared for Accelerator

183   Mass Spectrometry (AMS) radiocarbon (^{14}C) dating at the Keck Carbon Cycle AMS laboratory

184   at UC Irvine (KCCAMS). Authigenic carbonate samples were subsampled to isolate the cement

185   and groundmass components. Carbonate from the mussel shells was analyzed both as a

186   homogenized powder as well as shell fragments. To test for potential contamination by

187   secondary aragonite or calcite, duplicates were performed on samples treated with 10% HCl.

188

189   The carbonate samples were hydrolyzed to CO_2 in individual reaction chambers, evacuated,

190   heated and acidified with orthophosphoric acid at 90°C. The resultant CO_2 was converted to

191   graphite using an iron catalyst and the hydrogen reduction method (Vogel et al. 1987). Sample

192   preparation backgrounds have been subtracted, based on measurements of ^{14}C-free calcite and

193   oxalic acid I. All ^{14}C results were corrected for isotopic fractionation according to the

194   conventions of Stuiver and Polach (1977) with δ^{13}C values measured on prepared graphite using

195   the AMS spectrometer. Radiocarbon concentrations are given as Δ^{14}C and conventional

196   radiocarbon age following Stuiver and Polach (1977).

197

198   2.6 U-Th age dating of authigenic carbonates

199   U-Th dating of authigenic carbonates was carried out at the NERC Isotope Geosciences

200   Laboratory, British Geological Survey. Samples were processed via total dissolution techniques,

201   with isotope ratios measured on a Thermo Neptune Plus multi-collector ICP-MS, relative to a

202   mixed ^{229}Th-^{236}U tracer calibrated against gravimetric solutions of CRM 112a U and Ames

203   laboratory high purity Th. Details of the analytical protocol are provided in the Supplementary

204   Material. U-Th age calculations were performed using an in-house Excel spreadsheet, and are

205   calculated using the decay constants of Cheng et al. (2013).

206

207 **3. Results**

208 3.1 X-Ray diffraction and petrography

209 Calcium carbonate ($CaCO_3$) dominates the authigenic carbonate samples (48-97%) but not the

210 surrounding sediment (3-14%) (Table 1). Aragonite accounts for more than 60% of the

211 groundmass and up to 99% of the carbonate cement, with secondary amounts (< 15%) of low

212 and high-Mg calcite present, creating an aragonite-cemented intraclast breccia at both sites (Fig.

213 S1). The detrital fraction consists of poorly sorted accessory minerals, such as quartz, feldspar,

214 plagioclase, and pyroxene that are supported in a matrix of clay to silt-size particles, consistent

215 with grain size from the surrounding sediment.   The clasts are sub-rounded to very angular,

216 particularly in the Baltimore Canyon specimen (Fig. 4). Voids between intraclasts and bivalve

217 shells are completely or partially filled with fibrous or bladed aragonite, showing multiple

218 generations of mineral growth. Fractures intersect well-developed radiating crystals of aragonite

219 in the Baltimore Canyon sample. Bioclasts are observed in both samples, either as intact shells,

220 aragonite filled, or skeletal molds. The organic carbon (C_{org}) content of the authigenic carbonate

221 groundmass and cement was less than 0.4%, whereas the sediment, especially at the Norfolk

222 seep site, had higher %C_{org} (Table 1). The shell carbonate was dominated by both aragonite

223 and/or calcite with $CaCO_3$ ranging between 95 to 97%.

224

225 3.2 Strontium isotopes

226 The strontium isotope ($^{87}Sr/^{86}Sr$) compositions of the authigenic carbonates and mussel shells

227 were investigated to constrain the fluid source and flow pathway for carbonate precipitation

228 (Sample et al., 1993). $^{87}Sr/^{86}Sr$ ratios for the authigenic carbonates, mussel shells, and water

229   samples ranged from 0.70915 to 0.70924 (Tables 1 and 2). The average authigenic carbonate

230   (n=4) and mussel shell (n=2) $^{87}Sr/^{86}Sr$ ratios at both sites were equivalent, $0.70920 \pm 3x10^{-5}$ and

231   $0.70920 \pm 2x10^{-5}$, respectively. In comparison, the average seawater (n=6) $^{87}Sr/^{86}Sr$ ratio was

232   $0.70917 \pm 2x10^{-5}$ but was not statistically different (Student T-test; p>0.05) from the authigenic

233   carbonate and shell samples.

234

235   3.3 Stable carbon, oxygen, and sulfur isotopes

236   At Norfolk, shells from both living and dead mussels yielded average $\delta^{13}C$ values of -2.59 $\pm$

237   1.68‰ (n=34) and -7.10 $\pm$ 3.20‰ (n=16), respectively, and an average $\delta^{18}O$ value of 3.71 $\pm$

238   0.25‰ (n=34) and 3.82 $\pm$ 0.39‰ (n=16), respectively (Table 2). No statistical difference

239   (Student's t-test, P>0.05) exists between shell $\delta^{18}O$ values from dead and living specimens;

240   however, shells from living mussels were significantly enriched in ^{13}C relative to shells from

241   dead specimens (Student's t-test, P<0.05). Only shells from live mussel specimens were

242   analyzed from the Baltimore Canyon seep site and yielded average shell $\delta^{13}C$ and $\delta^{18}O$ values of

243   and -6.84 $\pm$ 1.97‰ and 2.57 $\pm$ 0.28‰ (n=30), respectively. At both sites, the shell $\delta^{13}C$ values

244   were lighter relative to bottom water dissolved inorganic carbon (DIC) $\delta^{13}C$ values (0.90±0.05;

245   n=2), but heavier relative to the Baltimore Canyon methane $\delta^{13}C$ value (-68‰; Pohlman et al.,

246   2015). Compared to shells from Norfolk, mussel shell isotope values from Baltimore Canyon

247   were heavier in $\delta^{13}C$ and $\delta^{18}O$ by ~4‰ and ~1‰, respectively. At both sites, shells $\delta^{18}O$ were

248   enriched in ^{18}O relative to ambient seawater, where bottom water $\delta^{18}O$ values from Norfolk and

249   Baltimore canyons were 0.34 and 0.53‰, respectively.

250

251   Shell isotopic variability over the lifespan of an individual specimen was calculated as the

252   standard deviation of 8 to 12 stable isotope values from material collected along a transect from

253   the umbo to the ventral margin (Fig. S2). Individual lifespan variability ranged from 0.11 to

254   0.56‰ and 0.69 to 3.57‰ for shell $\delta^{18}O$ and $\delta^{13}C$ values (n=13), respectively. On average, the

255     $\delta^{18}O$ and $\delta^{13}C$ variability over the mussel lifespan was 0.24 and 1.49‰, respectively. Lifespan

256   variability represented less than 10% of the average shell $\delta^{18}O$ signature at both sites, but up to

257   42% of the average shell $\delta^{13}C$ signal at the Norfolk seep site and 21% at the Baltimore Canyon

258   seep site. The mussel periostracum $\delta^{13}C$ signature from samples collected at Norfolk seep field

259   ranged from -70.66 to -29.92‰ (n=40), with an average value of -56.99±12.85‰ (Table 2).

260   Mussel periostracum from Baltimore Canyon was not analyzed since sample preservation in

261   ethyl alcohol precluded reliable $\delta^{13}C$ results.

262

263   The average $\delta^{13}C$ signature of the bulk authigenic carbonate from Norfolk and Baltimore

264   canyons was -45.51±1.66‰ (n=5) and -48.43 ±1.02‰ (n=4), respectively. However, in

265   comparison to the cement, the groundmass $\delta^{13}C$ values were heavier by 1-3‰ (Table 1). The

266   bulk $\delta^{18}O$ values were similar, 3.80 ±0.05‰ (Norfolk, n=5) and 3.95±0.47‰ (Baltimore

267   Canyon, n=4) with < 1‰ difference between the groundmass and cement at both sites (Table 1).

268   The authigenic carbonate $\delta^{18}O$ values were heavier by ~3‰ relative to bottom water $\delta^{18}O$ values.

269

270   Sulfur ($\delta^{34}S$) isotopes were analyzed from *Bathymodiolus* sp. gill tissues collected at each seep

271   field. Gill $\delta^{34}S$ values ranged from -4.07 to 21.55‰ (Table 3), with no statistical difference

272   between the sites (Student's t-test, P>0.05); however, gill $\delta^{34}S$ values at Baltimore Canyon

273   displayed a larger range compared to the Norfolk seep, from -4.07 to 18.13‰ (n=20) versus 8.65

274   to 21.55‰ (n=23).   Periostracum $\delta^{34}S$ values from the Norfolk seep were similar to gill $\delta^{34}S$

275   values, ranging from 8.82 to 22.65‰, averaging 16.63±4.01‰ (n=28). Seep sediment $\delta^{34}S$

276   values averaged 5.53±2.16‰ (n=4) at Norfolk and 2.42±3.6‰ (n=5) at Baltimore Canyon

277   (Table 3).

278

279   3.4 Radiocarbon (^{14}C) analysis

280   The $\Delta^{14}C$ signatures of the authigenic carbonates were significantly depleted in ^{14}C, ranging from

281   -959‰ to -740‰ with corresponding ^{14}C ages of 25,570±210 to 10,770±35 ^{14}C years (Table 4).

282   The ^{14}C ages of mussel shells on the seabed were younger relative to the authigenic carbonate

283   age. The ^{14}C age of the mussel shells derived from living specimens varied from 905±20 to

284   1,935±20 ^{14}C years, and the average ^{14}C age of the mussel shells derived from dead specimens at

285   Norfolk was 1,345±20 ^{14}C years (Table 4). There was no statistical difference (Student's T-test,

286   P>0.05) between shell from dead specimens that were pretreated with 10% HCl and those left

287   untreated (Table 4), yielding an average ^{14}C age of 1,180 ^{14}C years, indicating that secondary

288   aragonite and calcite are negligible.

289

290   3.5 U-Th age calculation

291   Discrete subsamples of late-stage cavity-filling authigenic carbonate weighing between 4.1-17.2

292   mg were hand-drilled from two hand specimens collected from the Baltimore (n=5) and Norfolk

293   Canyon (n=5) sites (Fig. 4). These were analysed along with 9 detritus samples (5 from Norfolk

294   and 4 from Baltimore Canyon) consisting of material loosely adhering to the outside surfaces of

295   the hand specimens, and material recovered from the base of push cores collected within 2 km of

296   the authigenic carbonates.   Tabulated results are reported in Table 5.   Authigenic carbonate

297   cement samples contained 3.2 to 4.6 ppm U, and 0.06 to 0.59 ppm Th. $^{230}Th/^{232}Th$ activity ratios

298   were between 2.2 and 8.6, clustering towards the lower end of the range reported from other

299   occurrences of methane-related authigenic carbonates (e.g., Teichert et al. 2003; Bayon et al.

300   2009; Fig. S3 A). The implication is that the analysed authigenic carbonates incorporate detrital

301   material, such as clay minerals, which carry ^{232}Th, and an associated amount of initial ^{230}Th.

302   Since initial ^{230}Th is not related to the in-situ decay of ^{234}U, a correction is required in order to

303   calculate a robust carbonate precipitation age.   The presence of initial ^{230}Th is typically

304   addressed via (i) leaching techniques aimed at separating the carbonate and detrital components

305   of a sample in order to calculate a two-point isochron age (e.g. Teichert et al., 2003; Berndt et al.,

306   2014), or total dissolution of the samples, with detrital corrections based on either (ii) a

307   theoretical detritus composition which assumes secular equilibrium in the ^{238}U decay chain, and

308   a $^{232}Th/^{238}U$ ratio linked to average continental crust composition (e.g. Aharon et al., 1997; Feng

309   et al., 2010; Liebetrau et al., 2014), or (iii) a measured, site-specific detrital isotopic composition

310   (e.g. Teichert et al., 2003; Bayon et al., 2009; 2015). Initial ^{230}Th in marine authigenic carbonates

311   is likely to be a mixture of ^{230}Th incorporated within the detrital material and hydrogenous ^{230}Th

312   scavenged onto grain surfaces from the decay of ^{234}U in the water column, with the impact of the

313   latter increasing with water depth (Henderson and Anderson, 2003). Consequently, site-specific

314   corrections are likely to be more appropriate, particularly for samples collected at depths greater

315   than a few hundred meters. The impact of excess ^{230}Th scavenged from seawater is illustrated by

316   the measured $(^{230}Th/^{238}U)$ of the five detritus samples from the Norfolk Canyon site (depth of

317   ~1600 m), which range from 1.7 to 2.1 (Table 5), and are significantly higher than the secular

318   equilibrium value of 1. Conversely $(^{230}Th/^{238}U)$ values from the shallower Baltimore Canyon site

319   (depth ~385 m) are, as expected, lower (1.29-1.46) but still in excess of secular equilibrium.

320   Details of the average detrital U and Th compositions used to calculate corrected U-Th dates at

321   Baltimore Canyon and Norfolk Canyon are provided in the supplementary material.

322   The U-Th ages from the Norfolk seeps, corrected for initial detrital and hydrogenous ^{230}Th, range

323   from 1.0±0.7 ka to 3.3±1.3 ka (Table 5). In comparison, the corrected U-Th ages of the

324   Baltimore Canyon authigenic carbonate were older, ranging from 14.7±0.6 ka to 15.7±1.6 ka

325   (Table 5). Modelled initial $(^{234}U/^{238}U)_i$ values are statistically equivalent to the mean modern

326   seawater $(^{234}U/^{238}U)$ of 1.1466 (Robinson et al., 2004; Fig. S3 B), meaning that U incorporated in

327   the authigenic carbonates was sourced from seawater, rather than pore waters, which would be

328   comparatively enriched in ^{234}U (Henderson et al., 1999).

4. Discussion

329

330   4.1 Authigenic carbonate formation

331   The aragonite-dominated authigenic carbonates form pavements and/or irregular blocky build-

332   ups on the seafloor. The carbonates consist of bioclasts, organic matter, and angular clasts of

333   terrigenous origin. While the contemporary Baltimore Canyon does not connect with a river

334   system, rivers delivered a significant volume of sediment to the submarine canyons incising the

335   shelf during Pleistocene sea-level lowstands (e.g., Forde et al. 1981). The fluvial influence on

336   the canyons is observed in both the geomorphic features and grain size, where coarse to medium

337   grained, shelly terrigenous sands are observed adjacent to the canyon heads (Obelcz et al. 2014).

338   The similarity between neodymium isotope $(^{143}Nd/^{144}Nd)$ values from Baltimore Canyon surface

339   sediment (0.51208; Prouty et al., 2015) and Hudson River sediment (0.51206; Goldstein and

340   Jacobsen 1987) highlights past connectivity with proximal fluvial sources.

341

342   The authigenic carbonate texture may result from in-situ brecciation of weakly consolidated

343   sediment, possibly triggered by seismic and venting-induced disturbances, such as rapid

344   sedimentation related to episodic and rapid release of trapped fluids or gases (Matsumoto 1990).

345   Fractures cross cutting multiple generations of aragonite precipitate in the Baltimore Canyon

346   authigenic carbonate (Fig. 4) may signify past disturbance events. The dominance of aragonite

347   at both seep sites suggests precipitation at or close to the seafloor (see review in Suess 2014),

348   where sufficiently high sulfate concentrations inhibit high-Mg calcite crystallization (e.g.,

349   Bohrmann et al. 1998). This interpretation is consistent with carbonate $^{87}Sr/^{86}Sr$ and $\delta^{234}U$

350   isotope results that indicate precipitation from seawater-derived fluids (e.g., Naehr et al. 2007),

351   rather than deep-seated formation waters that are less radiogenic than modern seawater.

352

353   4.2 Anaerobic oxidation of methane

354   The main driver of authigenic carbonate precipitation at or near the sediment interface is

355   anaerobic oxidation of methane (AOM) via sulfate reduction ($CH_4 + SO_4^{2-} \rightarrow HCO_3^- + HS^- + H_2O$).

356   This reaction drives an increase in pore water alkalinity by the production of biocarbonate

357   (HCO_3^-) and favors carbonate precipitation. Carbonate precipitation from methanogenesis can

358   also occur deeper in the sediment column (e.g., Orphan et al. 2004; Gieskes et al. 2005) and is

359   typically characterized by carbonate $\delta^{13}C$ values > -40‰ (Aharon et al. 1997).   However,

360   authigenic carbonate $\delta^{13}C$ values from Norfolk and Baltimore canyons are lighter (-45 to -48‰),

361   in agreement with $\delta^{13}C$ values at cold seep sites where microbial AOM is the dominant driver of

362   authigenic aragonite precipitation.   The heavier $\delta^{13}C$ values of the authigenic carbonates

363   compared to methane represent the incorporation of seawater DIC that is relatively enriched in

364   ^{13}C.   Results of a two end-member $\delta^{13}C$ mixing model yield a contribution from methane-

365   derived carbon of ~70%, with the remaining ~30% attributed to seawater DIC-derived carbon

366   precipitated near the sediment-water interface. Furthermore, $\delta^{13}C$ values of AOM-related lipids

367   extracted from the authigenic carbonates were strongly depleted in ^{13}C, (i.e., archaeol: -74.3‰;

368   Campbell et al., 2015), confirming the dominance of microbial methane as the dominant carbon

369   source for the Archaea. The authigenic carbonate $\delta^{13}C$ and $\delta^{18}O$ values are also consistent with

370   Group I carbonates that typify carbonate precipitation of microbial origin within the uppermost

371   few centimeters below the sediment-water interface (Joseph et al. 2013).

372

373   In addition to AOM, sulfate reduction is also a dominant process that occurs in methane-rich

374   sediments, resulting in sulfur fractionation in the pore water and sediment. Sulfate reduction

375   may therefore explain the light surface sediment $\delta^{34}S$ values (from -2.62 to 8.20‰; Table 3)

376   relative to seawater sulfate (+20‰; Heyl et al. 2007). The resulting hydrogen sulfide can then be

377   used to support the metabolic processes of surrounding chemosynthetic communities. For

378   example, Van Dover et al. (2003) reported that the mussel *B. heckerae* collected from Blake

379   Ridge derive up to 25% of their organic sulfur from sulfide. Using a two end-member mixing

380   model with a H_2S $\delta^{34}S$ value of -10‰, and the average *Bathymodiolus* sp. gill $\delta^{34}S$ values from

381   each seep site, the reliance on H_2S as an energy source at Norfolk and Baltimore canyon seep

382   fields was estimated at 16% and 14%, respectively. However, variable gill $\delta^{34}S$ values indicate

383   uptake of up to 80% of H_2S (i.e., gill $\delta^{34}S$ value of -4.07‰ at the Baltimore Canyon Seep site),

384   suggesting free-living and/or symbiotic thiotrophic bacteria may play a nutritional role at the

385   base of the food web (Yamanaka et al. 2003). As an alternative to mussel tissue isotopic studies,

386   the mussel shell periostracum derived from both living and dead specimens represents a valuable

387   source of information about the seep environment. The similarity between the periostracum and

388   mussel gill $\delta^{34}S$ values from Norfolk suggests a high degree of nutrient flow between the soft

389   tissue, allowing for greater fidelity in using periostracum isotopic ratios in place of respirable

390   tissues of living specimens.   This is particularly essential when mussel tissue is not available,

391   such as with archived specimens or those at quiescent vent sites.

392

393   4.3 Estimation of fluid composition and age

394   The composition of the seeping fluids can also be characterized by the mussel shell $\delta^{13}C$ values,

395   with differences between the living and dead specimens reflecting changes in the flux of methane

396   in the past, or possibly a change in the composition of the seeping fluids. At both sites, the shell

397   carbonate and periostracum $\delta^{13}C$ values were lighter relative to bottom water DIC $\delta^{13}C$ values

398   (Table 2).   This difference suggests an additional carbon source for shell calcification, and

399   illustrates the decoupling between calcification and metabolic pathway (Aharon et al. 1997). The

400   light periostracum $\delta^{13}C$ values (-57‰; Table 2) agree with previous work concluding that mussel

401   shell periostracum originates from dietary sources, and is an alternative to soft tissue for trophic

402   studies (Geist et al. 2005). Assuming a regional methane $\delta^{13}C$ value of -68‰ (Pohlman et al.,

403   2015), the average percent contribution of methane to shell calcification was estimated at 11% at

404   Baltimore Canyon and 5% at Norfolk.   However, shell $\delta^{13}C$ values from dead specimens

405   collected at Norfolk indicate a temporal shift in seepage activity and/or composition of seeping

406   fluids. Specifically, a reduction in $\delta^{13}C$ values of up to 17‰ observed in the dead specimens is

407   equivalent to a ~25% increase in methane contribution to shell calcification.   Comparison of

408   relative ^{14}C-derived ages from the dead and live specimens suggests this change could have

409   occurred within a few centuries (<500 years) (Table 4).

410

411   Carbonate shell $\delta^{13}C$ variability also has the potential to record environmental changes such as

412   changes in fluid source, as well as fluid-venting activity over the lifespan of the mussels (e.g.,

413   Lietard and Pierre 2008). Although the precise chronology of the variability is unknown because

414   of the difficulty in dating the specimens, estimates of ages of *B. brevior* and *B. thermophiles*

415   range from 18 to more than 25 years (Schöne and Giere 2005).   Therefore, lifespan $\delta^{13}C$

416   variability reported above may be related to changes in methane flow within several decades.

417   The spatial distribution of living and dead mussels may also imply changing fluid composition or

418   flux rates, as suggested by Van Dover et al. (2003) from HOV dives on the Blake Ridge Diapir.

419

420   The shell carbonate $\delta^{18}O$ isotopic signature at Norfolk overlap with both *Bathymodiolus* and

421   *Calyptogena* shell samples from other cold seeps (Lietard and Pierre 2008). In comparison,

422   Baltimore Canyon shell $\delta^{18}O$ values are lighter, reflecting warmer in-situ temperatures (~9°C)

423   relative to the deeper, colder in-situ temperatures (~4°C) at Norfolk. Using bottom water $\delta^{18}O$

424   values from Baltimore and Norfolk canyons, the predicted carbonate $\delta^{18}O$ value precipitated at

425   equilibrium yields heavier carbonate $\delta^{18}O$ values relative to measured shell values from

426   Baltimore and Norfolk by 0.68 and 0.42‰ respectively. Therefore, there is evidence of isotopic

427   disequilibrium, indicating the influence of ^{18}O-poor water and/or warmer seeping fluids (e.g.

428   Lietard and Pierre 2008). As a result, the predicted seawater temperatures using an aragonite

429   paleotemperature equation of Grossman and Ku (1986) are warmer by 1-3°C compared to

430   contemporary in-situ temperatures, a difference at least three times greater than the $\delta^{18}O$-derived

431   temperature analytical uncertainty of 0.28°C.

432

433   The influence of methane is also captured in the light carbonate Δ^{14}C values and relatively old

434   ^{14}C-derived ages of mussel shells from living specimens.   Seawater samples collected near the

435   Norfolk seep field yield an average DI^{14}C value of -24.17±0.6‰, consistent with seawater Δ^{14}C

436   values from below the mixed layer depth in Norfolk Canyon. In contrast, the average mussel

437   shell Δ^{14}C value from living specimens from the Norfolk seep field is -115±3‰. Assuming a

438   methane Δ^{14}C signature of -880‰ (<0.12 pMC; Pohlman et al. 2009) and a DIC Δ^{14}C signature

439   of -24‰ (this study), ~10% of the carbon signature for shell calcification is derived from fossil

440   carbon. As a result, the contribution from fossil carbon can yield a false ^{14}C carbonate age (e.g.,

441   Aharon et al. 1997). The dilution from fossil carbon may result in over prediction of ^{14}C-derived

442   ages by 5 to 11%.

443

444   Owing to this incorporation of fossil carbon, we expect a disparity between the ^{14}C-derived age

445   of the authigenic carbonates and the independently derived U-Th age. The average Δ^{14}C

446   signatures of the authigenic carbonates at both sites are significantly depleted in ^{14}C, with values

447   ranging from -894‰ to -878‰ and corresponding ^{14}C ages ranging from 17.99 to 19.35 ka.   In

448   comparison, average U-Th ages from the Norfolk and Baltimore canyon seep sites were 1.0-3.3

449   ka and 14.7-15.7 ka, respectively. Thus, the disparity between the ^{14}C and U-Th derived ages is

450   a few thousand years at the Baltimore Canyon seep but at least 13 ka at the deepwater Norfolk

451   seep. The differences between the ^{14}C and U-Th ages are probably a complex function of

452   absolute age of the authigenic carbonates, methane flux, and the ^{14}C signature of the source

453   methane, and the results may imply greater incorporation of fossil carbon in the authigenic

454   carbonates at Norfolk Seep.

455

19

456   4.4 Formation model and paleoenvironment

457   The U-Th ages from methane derived authigenic carbonates indicate that hydrocarbon seepage

458   related to the formation of those carbonates occurred at the Baltimore Canyon seep field toward

459   the end of the Late Pleistocene, and was more recent (Holocene) at the Norfolk seep field. These

460   are the first absolute dates for the timing of hydrocarbon seepage along the US Atlantic margin,

461   and although the limited nature (single samples at two sites) these ages are supported by

462   additional U-Th dating conducted on more recently obtained authigenic carbonate samples along

463   the US Atlantic margin (Condon et al., 2015). Nonetheless, the origin of seeps and gas expulsion

464   geomorphic features (e.g., pockmarks and "gas blowouts") along the US Atlantic Margin

465   remains uncertain.

466

467   The occurrence of gas seeps and pockmarks associated with fluid expulsion at depths less than

468   500 m, which are outside the methane hydrate stability field, may have a microbial origin from

469   in-situ bacterial decay of organic matter or updip migration of gases produced by the same

470   process or released from methane hydrate dissociation at greater water depths on the upper slope

471   (Skarke et al. 2014). Such expulsion may also have a thermogenic origin at depth (Hill et al.

472   2004; Newman et al. 2008; Brothers et al. 2014). However, the geochemical analyses presented

473   here yield carbonate δ^{13}C values < -40‰. When coupled with observations by Pohlman et al.

474   (2015) of -68‰ in the bottom waters, a thermogenic origin for the methane is precluded. This

475   agrees with earlier work by Newman et al. (2008) that demonstrated the microbial origin of pore

476   fluid DIC δ^{13}C values along the US mid-Atlantic shelf break. Hill et al. (2004) argued that

477   microbial gas flowing updip from dissociating gas hydrates is responsible for the distribution of

478   gas blowouts in the region, and Skarke et al (2014) make the same argument for the distribution

479   of hundreds of seeps on the continental slope updip of the present-day hydrate stability limit,

480   particularly on the mid-Atlantic part of the margin. Recent multi-channel seismic profiles on the

481   upper continental slope below the Baltimore Canyon seep field do not reveal clear evidence for

482   strata that could be laterally channeling gas updip into the seeps (Ruppel et al., 2015b), but these

483   observations are equivocal.

484

485   An alternate explanation for the presence of the Baltimore Canyon seeps at ~400 m water depth

486   is that overpressures have accumulated within thick, rapidly deposited Pleistocene sediments,

487   leading to vertical fluid and gas expulsion (Brothers et al. 2014). Studies on passive margins

488   offshore Europe and Asia have also advanced this explanation for focused fluid flow in areas of

489   high sedimentation rates under excess pore pressure (Berndt 2005). This interpretation is

490   consistent with the non-aquifer model of Dugan and Flemings (2002), where rapid sediment

491   loading during the Pleistocene sea-level lowstand created overpressure gradients, forcing fluids

492   to migrate upward and outward toward the seafloor. During the Pleistocene, significant volumes

493   of sediment were delivered to the outer shelf, with much of it transported directly into shelf-

494   sourced canyons and then offshore to deep-sea fans (e.g., Poag 1992). The fluvial influence on

495   the canyons is observed in both the geomorphic features and grain size, where coarse to medium

496   grained, shelly terrigenous sands are observed adjacent to the canyon heads (Obelcz et al. 2014).

497   The Mid-Atlantic region is also marked by a seaward thickening wedge of shelf edge delta

498   deposits (200-400 m thick) (Hill et al., 2004; D. Brothers et al., 2013). Along the New Jersey

499   continental slope for example, sedimentation rates rose sharply during Pleistocene sea-level

500   lowstand (Dugan and Flemings, 2002), with rates as high as 353 cm kyr^{-1} (McHugh and Olson,

501   2002). The age of the Baltimore Canyon authigenic carbonate further supports a link between

502   rapid loading by organic-rich sediment during the Pleistocene sea-level lowstand and subsequent

503   fluid flow from overpressure.   Such overpressures may also contribute to pervasive slope

504   instability on this part of the Mid-Atlantic margin (ten Brink et al., 2014).

505

506   Our analysis (Fig. 5) shows that the Baltimore seep field would have been outside the methane

507   hydrate stability field even between 14.7±0.6 ka to 15.7±1.6 ka. The ensuing Late Pleistocene to

508   Holocene sea-level rise increased hydrostatic pressure, which could move the seep field closer to

509   the hydrate stability condition under isothermal conditions.   However, dramatic bottom water

510   warming between the presumed cold Late Pleistocene temperature and the ~9°C observed in

511   2013 from in-situ temperature measurements overwhelms the impact of increased pressure. The

512   Baltimore Canyon seep field may now or in the past have emitted migrated methane that was

513   released by gas hydrate dissociation at greater water depths; however in-situ gas hydrate

514   dissociation is clearly ruled out as the source of methane emissions. This regime contrasts with

515   the hydrate-controlled methane venting off Svalbard, where seasonal fluctuations in bottom

516   water temperatures cause variable gas hydrate dissociation at a depth between 380 to 400 m

517   (Berndt et al., 2014).

518

519   The driving mechanism for methane venting the Norfolk seep field (~1600 m) is more difficult

520   to explain since the seep is well inside the gas hydrate stability zone and there is no underlying

521   salt diapir.   Skarke et al. (2014) postulated that the Norfolk seep field is fed by gas flowing

522   through fractured Eocene rock, but a clear triggering mechanism that could explain seepage

523   consistent mid-Holocene U-Th date of the authigenic carbonates is lacking.   Recent high-

524   resolution seismic imaging by the USGS shows fractures channeling methane to the seep sites

525   from hundreds of meters below the seafloor (Ruppel et al., 2015a).   Despite the inferred deep

526   source of some of the methane, it is notable that the $\delta^{13}C$ data still support an entirely microbial

527   origin for the gas. There is evidence at both sites of upward flux of methane that is isotopically

528   similar between the sites with respect to carbon, most likely linked to long-term accumulation,

529   compaction, and over-pressuring of organic-rich sediment. This can occur when the intense

530   methane fluxes move the sulfate-methane transition zone (SMTZ) very close to the seafloor

531   (Orcutt et al., 2011).

532

533   4.5 Relationship to Global Setting

534   A variety of driving mechanisms has been proposed to explain methane venting at cold seeps,

535   including hydrological and tidal pumping, warming of bottom water (Suess 2014), excess pore

536   pressure in areas of high sedimentation along the passive margins of Europe and Africa (Berndt

537   2005), seismic activity (e.g., Fischer et al., 2013), and links to sea-level lowstands (e.g., Teichert

538   et al., 2003; Feng et al., 2010; Liebetrau et al., 2010). In many of these cases, a major mechanism

539   for methane release is a change in hydrostatic pressure and/or temperature, and subsequent

540   hydrate dissociation, as in the case of the South China Sea (Han et al., 2014) and Svalbard

541   (Westbrook et al., 2009; Berndt et al., 2014). Even with the assumption of very cold bottom

542   water temperatures, the Baltimore seep field would have been outside the methane hydrate

543   stability field at ~15ka (Fig. 5), meaning that in-situ gas hydrate dissociation cannot have ever

544   contributed to methane emissions there since the Late Pleistocene. Despite observations of

545   numerous landslide scars in the Baltimore Canyon landslide zone (ten Brink et al. 2014), ages

546   that could constrain the timing of slide events are are not available close to the seep site.   The

547   ages farther downslope at the base of hemipelagic sediment overlying the youngest mass

548   transport deposit range between 5200 ± 150 and 10,080 yr BP (Embley, 1980).   While these

549   dates are several thousand years younger than the age of the authigenic carbonate samples

550   analyzed from the Baltimore Canyon seep field site, the slide material that was dated is probably

551   not related to sediments originally at the top of the ridge where the seep field is located.   For

552   now, we can only postulate that other passive margins with similar depositional regimes similar

553   to that of the northern US Atlantic margin may also be the loci of widespread and as-yet

554   undiscovered seepage that can be traced to similar mechanisms of overpressure accumulation

555   and eventual fluid expulsion, possibly with a slide-related connection.

556

557   **5. Conclusion**

558   The geochemistry, mineralogy, and petrology of authigenic carbonates and mussel shells

559   collected from two seep sites along the mid-Atlantic portion of the USAM in a newly-discovered

560   seep province provide the first direct information about methane sources, the processes driving

561   carbonate precipitation and chemosynthetic processes, and the nature of fluid-rock interaction.

562   Taken together, the $\delta^{234}U$, $^{87}Sr/^{86}Sr$, $\delta^{13}C$ and $\Delta^{14}C$ values support shallow precipitation of

563   aragonite driven by AOM and at equilibrium with seawater. At the deepwater Norfolk seep,

564   comparison of shell $\delta^{13}C$ values from dead and living specimens indicates a temporal shift in

565   seepage activity and/or composition of seeping fluids. Comparison between shell $\delta^{13}C$ values of

566   living versus dead specimens from Norfolk suggests a ~25% increase in methane contribution

567   within several centuries. In addition, changes in shell $\delta^{13}C$ values during growth may be related

568   to changes in methane flow throughout the organisms' lifespan (<25 years). The range of mussel

569   gill and periostracum $\delta^{34}S$ values from both sites suggests an admixture of sulfur sources,

570   hydrogen sulfide (H_2S) and seawater sulfate (SO_4), with the former sourced from sulfate

571   reduction during AOM. Lighter mussel shell $\Delta^{14}C$ values highlight dilution of the ^{14}C pool with

572　fossil carbon. As a result, authigenic carbonate ^{14}C- and U-Th-derived ages are discordant.

573　According to U-Th ages, methane seepage is thought to have occurred at the uppermost slope

574　Baltimore Canyon seep field toward the end of the Pleistocene (14.7±0.6 ka to 15.7±1.6 ka) and

575　between 1.0±0.7 ka to 3.3±0.1.3 ka at the deepwater Norfolk seep field. Fluid flow from the

576　thick pile of overpressured Pleistocene sediments deposited at the sea-level lowstand is the most

577　likely mechanism to explain sustained methane venting at Baltimore Canyon, whereas venting

578　fluids at the Norfolk seeps, which are located well within the GHSZ, can be explained by flow

579　through fractured strata (Skarke et al. 2014; Ruppel et al., 2015a). At neither seep field does the

580　carbonate geochemistry support deep-sourced fluid of thermogenic origin. Instead, the isotope

581　and mineralogy of the carbonates indicate that microbial degradation of sedimentary organic

582　matter is the common source of widespread methane both outside (Baltimore Canyon) and well

583　within (Norfolk seep) the GHSZ. Results from this geochemical study, coupled with the

584　geophysical data of Skarke et al (2014) showing the distribution of seeps along the USAM,

585　highlights the potential role of the sedimentary framework in widespread venting at upper slope

586　locations updip of the current limit of gas hydrate stability. We postulate that high sedimentation

587　rate passive margins dominated by siliciclastic deposition due to glacial and fluvial processes

588　may have accumulated overpressures and produced episodes of fluid expulsion particularly

589　during Late Pleistocene lowstands. This implies that undiscovered methane seep provinces may

590　be widespread on upper continental slopes, which would have implications for carbon cycling

591　from the seafloor to overlying ocean-atmosphere system.

607

608

609   **Figure Captions**

610   **Figure 1**

611   Location map showing the Norfolk and Baltimore Canyon seep fields (green circles) relative to

612   the major shelf-break canyons (Norfolk, Washington, and Baltimore). The blue triangle outlines

613   the study area for the multi-disciplinary "Atlantic Deepwater Canyons" study.

614

615   **Figure 2**

616   (A) Baltimore Canyon, with the seep field located on the southern promontory overlooking the

617   canyon. The green circle denotes the seep that was sampled for mussel shells and authigenic

618   carbonates within the seep field. (B) Close-up view of shaded relief at the Baltimore Canyon

619   seep field, with bathymetric contours at 100 m spacing. The green circle denotes the seep that is

620   the focus of this paper. Red and orange circles are seeps from the Skarke et al. (2014) database

621   and from USGS water-column imaging surveys in April 2015, respectively. Some of the orange

622   and red seeps may correspond to the same location within the resolution of the data. Yellow

623   symbols are pockmarks mapped by Brothers et al. (2014). (C) Left: In-situ photo of deep-sea

624   mussel field of *Bathymodiolus* sp. Right: In-situ photo of deep-sea Cusk fish, *Brosme brosme*,

625   beneath authigenic pavement in soft substrate with low live mussel cover (D) Target strength

626   calculated from water column imagery collected with a Simrad EK60 using a 38 kHz transducer

627   during USGS surveys across the seep field in September 2015. The current deflects the plumes

628   slightly southeast in the water column. The analysis used the approach and software described in

629   Veloso et al. (2015).

630

631   **Figure 3**.

632   (A) Norfolk deep seep field, showing the locations of seeps in the Skarke et al. (2014) database

633   (red circles) and the sampled seep for authigenic carbonate and mussels as a green circle. (B)

634   Close-up of the Norfolk seep field, using the same key as in (A). (C) NOAA image of the

635   plumes emanating from the seep field in 2013, with the seep sampled for this paper indicated in

636   yellow. (D) Left: In-situ photo of dense deep-sea mussel field of live *Bathymodiolus* sp. on

637   irregular blocky build-up on the seafloor. Right: In-situ photos of live *Bathymodiolus* sp. at

638   active seep site with visible bubble stream.

639

640   **Figure 4**

641 Photographic and petrographic thin section images (plane polarized light; 40x) of the authigenic

642 carbonates sampled at the Norfolk seep site (dive NF-2012-14) and Baltimore Canyon seep site

643 (dive RB-2013-682). Infilling of voids by acicular aragonite, detrital grains, organic matter, and

644 bioclasts are noted in the matrix-supported clay to silt-size aragonite-dominated breccia.

645 Locations of sampling sites for U-Th dates (red squares) and radiocarbon (yellow squares) are

646 shown for their respective locations and corresponding sample number from Tables 4 and 5.

647

648 **Figure 5**

649 The evolution of Baltimore Canyon (squares) and Norfolk (circles) seeps in depth-temperature

650 (P-T) space relative to the methane hydrate stability field calculated with seawater

651 salinity. Closed symbols are present-day depth and temperature, and open symbols denote

652 estimated conditions at 15.1±1.6 ka and 3±1 ka, respectively.

653

654

655 **References**

656 Aharon P, Schwarcz HP, Roberts HH (1997) Radiometric dating of submarine hydrocarbon seeps in the Gulf of
657   Mexico. Geol Soc Am Bull 109:568-579
658 Bayon G, Henderson GM, Bohn M (2009) U–Th stratigraphy of a cold seep carbonate crust. Chem Geol 260:47-56
659 Bayon G, Henderson GM, Etoubleau J, Caprais J-C, Ruffine L, Marsset T, Dennielou B, Cauquil E, Voisset M,
660   Sultan N (2015) U-Th isotope constraints on gas hydrate and pockmark dynamics at the Niger delta margin. Mar
661   Geol 370:87-98
662 Berndt C (2005) Focused fluid flow in passive continental margins. Phil. Trans. R. Soc. A s 363:2855-2871
663 Berndt C, Feseker T, Treude T, Krastel S, Liebetrau V, Niemann H, Bertics VJ, Dumke I, Dünnbier K, Ferré B,
664   Graves C, Gross F, Hissmann K, Hühnerbach V, Krause S, Lieser K, Schauer J, Steinle L (2014) Temporal
665   Constraints on Hydrate-Controlled Methane Seepage off Svalbard. Science 343:284-287
666 Boetius A, Wenzhöfer F (2013) Seafloor oxygen consumption fuelled by methane from cold seeps. Nature Geosci
667   6:725-734
668 Bohrmann G, Greinert J, Suess E, Torres M (1998) Authigenic carbonates from the Cascadia subduction zone and
669   their relation to gas hydrate stability. Geology 26:647-650
670 Brothers LL, Van Dover CL, German CR, Kaiser CL, Yoerger DR, Ruppel CD, Lobecker E, Skarke AD, Wagner
671   JKS (2013) Evidence for extensive methane venting on the southeastern U.S. Atlantic margin. Geology 41:807-
672   810
673 Brothers DS, Luttrell KM, Chaytor JD (2013) Sea-level–induced seismicity and submarine landslide occurrence.
674   Geology 41:979-982

675 Brothers DS, Ruppel C, Kluesner JW, Brink US, Chaytor JD, Hill JC, Andrews BD, Flores C (2014) Seabed fluid
676   expulsion along the upper slope and outer shelf of the US Atlantic continental margin. Geophys Res Lett 41:96-
677   101
678 Campbell KA (2006) Hydrocarbon seep and hydrothermal vent paleoenvironments and paleontology: Past
679   developments and future research directions. Palaeogeogr. Palaeoclimatol. Palaeoecol. 232:362-407
680 Campbell PL, Prouty NG, Demopoulos, AWD, Roark, EB, Coykendall (2015) Lipid biomarkers and their specific
681   carbon isotopic composition from cold seep community authigenic carbonates and sediments from the Mid-
682   Atlantic Norfolk and Baltimore Canyons. Fall Meeting Amer. Geophys. Union, OS33A-2015.
683 Cheng H, Lawrence Edwards R, Shen C-C, Polyak VJ, Asmerom Y, Woodhead J, Hellstrom J, Wang Y, Kong X,
684   Spötl C, Wang X, Calvin Alexander Jr E (2013) Improvements in ^{230}Th dating, ^{230}Th and ^{234}U half-life values,
685   and U–Th isotopic measurements by multi-collector inductively coupled plasma mass spectrometry. Earth Planet
686   Sci Lett 371–372:82-91
687 Condon D, Sahy D, Ruppel C, Prouty N, Noble S, Team SP (2015) Tempo and longevity of methane efflux along
688   the US Atlantic margin. A Fall Meeting Amer. Geophys. Union, OS31B-07.
689 Dugan B, Flemings PB (2000) Overpressure and fluid flow in the New Jersey continental slope: implications for
690   slope failure and cold seeps. Science, 289, 288–9
691 Dugan B, Flemings PB (2002) Fluid flow and stability of the US continental slope offshore New Jersey from the
692   Pleistocene to the present. Geofluids 2:137-146
693 Duperron S, Guezi H, Gaudron SM, Pop Ristova P, Wenzhöfer F, Boetius A (2011) Relative abundances of
694   methane‐and sulphur‐oxidising symbionts in the gills of a cold seep mussel and link to their potential energy
695   sources. Geobiology 9:481-491
696 Embley RW (1980) The role of mass transport in the distribution and character of deep- ocean sediments with
697   special reference to the North Atlantic. Marine Geology 38, 23–50.
698 Feng D, Roberts HH, Cheng H, Peckmann J, Bohrmann G, Lawrence Edwards R, Chen D (2010) U/Th dating of
699   cold-seep carbonates: An initial comparison. Deep Sea Research Part II: Topical Studies in Oceanography
700   57:2055-2060
701 Fischer D, Mogollón JM, Strasser M, Pape T, Bohrmann G, Fekete N, Spiess V, Kasten S. (2013) Subduction zone
702   earthquake as potential trigger of submarine hydrocarbon seepage. Nature Geoscience. 1;6(8):647-51
703 .Forde EB, Stanley DJ, Sawyer WB, Slagle KJ (1981) Sediment transport in Washington and Norfolk submarine
704   canyons. Appl Ocean Res 3:59-62
705 Geist J, Auerswald K, Boom A (2005) Stable carbon isotopes in freshwater mussel shells: Environmental record or
706   marker for metabolic activity? Geochim Cosmochim Acta 69:3545-3554
707 Gieskes J, Mahn C, Day S, Martin JB, Greinert J, Rathburn T, McAdoo B (2005) A study of the chemistry of pore
708   fluids and authigenic carbonates in methane seep environments: Kodiak Trench, Hydrate Ridge, Monterey Bay,
709   and Eel River Basin. Chem Geol 220:329-345
710 Goldstein SJ, Jacobsen SB (1987) The Nd and Sr isotopic systematics of river-water dissolved material: implications
711   for the sources of Nd and Sr in seawater. Chem. Geol. (Isot. Geosci. Sect.) 66:245-272
712 Grossman E, Ku TL (1986) Oxygen and carbon isotope fractionation in biogenic aragonite: Temperature effects.
713   Isot Geosci 59:59-74
714 Han X, Suess E, Liebetrau V, Eisenhauer A, Huang Y (2014) Past methane release events and environmental
715   conditions at the upper continental slope of the South China Sea: constraints by seep carbonates. Int. J. Earth Sci.
716   103:1873-1887
717 Henderson GM, Anderson RF (2003) The U-series toolbox for paleoceanography. In Bourdon B, Henderson GM,
718   Lundstrom CC, Turner SP (eds) Uranium Series Geochemistry, Rev. Mineral. Geochem, 52:493-531
719 Henderson GM, Slowey NC, Haddad GA (1999) Fluid flow through carbonate platforms: constraints from
720   234U/238U and Cl- in Bahamas pore waters. Earth Planet. Sci. Lett. 169:99-111
721 Heyl TP, Gilhooly WP, Chambers RM, Gilchrist GW, Macko SA, Ruppel CD, Van Dover CL (2007)
722   Characteristics of vesicomyid clams and their environment at the Blake Ridge cold seep, South Carolina, USA.
723   Mar Ecol Prog Ser 339:169-184
724 Hill JC, Driscoll NW, Weissel JK, Goff JA (2004) Large‐scale elongated gas blowouts along the US Atlantic
725   margin. J. Geophys. Res., 109, B09101, doi:10.1029/2004JB002969.
726 Holden NE (1990) Total half-lives for selected nuclides. Pure Appl Chem 62(5):941-958
727 Hornbach MJ, Ruppel C, Saffer DM, Van Dover CL, Holbrook WS (2005) Coupled geophysical constraints on heat
728   flow and fluid flux at a salt diapir. Geophys Res Lett 32(24) doi: 10.1029/2005GL024862
729 Jaffrey A, Flynn K, Glendenin L, Bentley W, Essling A (1971) Precision measurement of half-lives and specific
730   activities of ^{235}U and ^{238}U, Phys. Rev. C, 4(5), 1889–1906,10.1103/PhysRevC.4.1889.

731 Joseph C, Campbell KA, Torres ME, Martin RA, Pohlman JW, Riedel M, Rose K (2013) Methane-derived
732   authigenic carbonates from modern and paleoseeps on the Cascadia margin: Mechanisms of formation and
733   diagenetic signals. Palaeogeogr. Palaeoclimatol. Palaeoecol. 390:52-67
734 Lietard C, Pierre C (2008) High-resolution isotopic records (δ^{18}O and δ^{13}C) and cathodoluminescence study of
735   lucinid shells from methane seeps of the Eastern Mediterranean. Geo-Mar Lett:195-203
736 Liebetrau V, Augustin N, Kutterolf S, Schmidt M, Eisenhauer A, Garbe-Schönberg D, Weinrebe W (2014) Cold-
737   seep-driven carbonate deposits at the Central American forearc: contrasting evolution and timing in escarpment
738   and mound settings. Int. J. Earth Sci. 103:1845-1872
739 Matsumoto R (1990) Vuggy carbonate crust formed by hydrocarbon seepage on the continental shelf of Baffin
740   Island, northeast Canada. Geochem J 24:143-158
741 McHugh CMG, Olson HC (2002) Pleistocene chronology of continental margin sedimentation:: New insights into
742   traditional models, New Jersey. Mar Geol 186:389-411
743 Naehr TH, Eichhubl P, Orphan VJ, Hovland M, Paull CK, Ussler Iii W, Lorenson TD, Greene HG (2007)
744   Authigenic carbonate formation at hydrocarbon seeps in continental margin sediments: A comparative study.
745   Deep Sea Res II 54:1268-1291
746 Newman KR, Cormier M-H, Weissel JK, Driscoll NW, Kastner M, Solomon EA, Robertson G, Hill JC, Singh H,
747   Camilli R (2008) Active methane venting observed at giant pockmarks along the US mid-Atlantic shelf break.
748   Earth Planet Sci Lett 267:341-352
749 NOAA (2012) NOAA explorers discover deepwater gas seeps off U.S. Atlantic coast. Press Release
750   (http://www.noaanews.noaa.gov/stories2012/20121219_gas_seeps.html)
751 Obelcz J, Brothers D, Chaytor J, Brink Ut, Ross SW, Brooke S (2014) Geomorphic characterization of four shelf-
752   sourced submarine canyons along the U.S. Mid-Atlantic continental margin. Deep Sea Res II 104:106-119
753 Olsson, IU (1970) The use of Oxalic acid as a Standard. In I.U. Olsson, ed., Radiocarbon Variations and Absolute
754   Chronology, *Nobel Symposium, 12th Proc.,* John Wiley & Sons, New York, p. 17.
755 Orcutt BN, Sylvan JB, Knab NJ, Edwards KJ (2011) Microbial ecology of the dark ocean above, at, and below the
756   seafloor. Microbiol Mol Biol Rev 75:361-422
757 Orphan VJ, Ussler W, Naehr TH, House CH, Hinrichs KU, Paull CK (2004) Geological, geochemical, and
758   microbiological heterogeneity of the seafloor around methane vents in the Eel River Basin, offshore California.
759   Chem Geol 205:265-289
760 Paull CK, Ussler W, Borowski WS, Spiess FN (1995) Methane-rich plumes on the Carolina continental rise:
761   Associations with gas hydrates. Geology 23:89-92
762 Poag CW (1992) U.S. Middle Atlantic Continental Rise: Provenance, Dispersal, and Deposition of Jurassic to
763   Quaternary Sediments. In: Poag CW, Graciansky PC (eds) Geologic Evolution of Atlantic Continental Rises.
764   Van Nostrand Reinhold, New York, pp100-156
765 Pohlman JW, Kaneko M, Heuer VB, Coffin RB, Whiticar M (2009) Methane sources and production in the northern
766   Cascadia margin gas hydrate system. Earth Planet Sci Lett 287:504-512
767 Pohlman, J., C. Ruppel, R. Colwell, S. Krause, T. Treude, M. Graw, M. Casso, L.-G. Boze, B. Buczkowki, and D.
768   Brankovits, 2015, Sediment and water column chemistry related to methane seepage along the northern US
769   Atlantic margin, Fall Meeting Amer. Geophys. Union, OS33A-1992.
770 Prouty , NG, Swarzenski, Mienis, F., Davies, A.J., Demopoulos, A., Condon, D. Ross, S, and Brooke, S. (2015)
771   Sources of Organic Matter to Deep-sea Corals Living in Submarine Canyons of the Mid-Atlantic Bight Region,
772   U.S. Aquatic Sciences ASLO Meeting, 27449
773 Quattrini AM, Nizinski MS, Chaytor JD, Demopoulos AWD, Roark EB, France SC, Moore JA, Heyl TP, Auster PJ,
774   Kinlan B, Ruppel C, Elliott KP, Kennedy BRC, Lobecker E, Skarke A, Shank T (2015) Exploration of the
775   Canyon-Incised Continental Margin of the Northeastern United States Reveals Dynamic Habitats and Diverse
776   Communities. PLoS ONE 10(10): e0139904. doi:10.1371/journal.pone.0139904
777 Robinson FL, Belshaw NS, Henderson GM (2004) U and Th concentrations and isotope ratios in modern carbonates
778   and waters from the Bahamas. Geochim. Cosmochim. Acta. 68:1777-1789
779 Ruppel C, Kluesner JW, Danforth W (2015a) Imaging Methane Seeps and Plumes on the U.S. Atlantic Margin
780   Sound Waves March June 2015. U.S. Geological Survey http://soundwaves.usgs.gov/2015/06/fieldwork3.html
781 Ruppel, C, Kluesner, JW, Pohlman J, Brothers D, Colwell F, Krause S. and Treude T. (2015b) Methane Hydrate
782   Dynamics on the US Atlantic Margin. DOE Fire-in-the -Ice 15(2): 10-13.
783 Sample JC, Reid MR, Tobin HJ, Moore JC (1993) Carbonate cements indicate channeled fluid flow along a zone of
784   vertical faults at the deformation front of the Cascadia accretionary wedge (northwest U.S. coast). Geology
785   21:507-510

786 Schöne BR, Giere O (2005) Growth increment and stable isotope variation in shells of the deep-sea hydrothermal
787   vent bivalve mollusk *Bathymodiolus brevior* from the North Fiji Basin Pacific Ocean. Deep Sea Res I 52:1896–
788   1910
789 Skarke A, Ruppel C, Kodis M, Brothers D, Lobecker E (2014) Widespread methane leakage from the seafloor on
790   the northern US Atlantic margin. Nature Geosci 7:657-661
791 Stuiver M, Polach HA (1977) Discussion reporting of ^{14}C data. Radiocarbon 19:355-363
792 Suess E (2014) Marine cold seeps and their manifestations: geological control, biogeochemical criteria and
793   environmental conditions. Int. J. Earth Sci. 103:1889-1916
794 Teichert BMA, Eisenhauer A, Bohrmann G, Haase-Schramm A, Bock B, Linke P (2003) U/Th systematics and ages
795   of authigenic carbonates from Hydrate Ridge, Cascadia Margin: recorders of fluid flow variations. Geochim
796   Cosmochim Acta 67:3845-3857
797 ten Brink US, Chaytor JD, Geist EL, Brothers DS, Andrews BD (2014) Assessment of tsunami hazard to the U.S.
798   Atlantic margin. Mar Geol 353:31-54
799 Van Dover CL, Aharon P, Bernhard JM, Caylor E, Doerries M, Flickinger W, Gilhooly W, Goffredi SK, Knick KE,
800   Macko SA, Rapoport S, Raulfs EC, Ruppel C, Salerno JL, Seitz RD, Sen Gupta BK, Shank T, Turnipseed M,
801   Vrijenhoek R (2003) Blake Ridge methane seeps: characterization of a soft-sediment, chemosynthetically based
802   ecosystem. Deep Sea Res I 50:281-300
803 Veloso M, Greinert J, Mienert J, De Batist M (2015), A new methodology for quantifying bubble flow rates in deep
804   water using splitbeam echosounders: Examples from the Arctic offshore NW-Svalbard. Limnol Oceanogr:
805   Methods, 13: 267–287. doi: 10.1002/lom3.10024
806 Vogel JS, Southon JR, Nelson DE (1987) Catalyst and binder effects in the use of filamentous graphite for AMS.
807   Nucl. Instr. Meth. Phys. Res. 29:50-56
808 Weinstein A, Navarrete L, Leonte M, Weber T, Ruppel C, Kellermann M, Arrington E, Valentine DL, Chepigin A,
809   Rosemore B, Green A, Du M., Scranton MI, Kessler JD (2016) Determining the flux of methane into the
810   Hudson Canyon at the edge of methane clathrate hydrate stability. Geophysical Research Letters, in review
811 Westbrook GK, Thatcher KE, Rohling EJ, Piotrowski AM, Pälike H, Osborne AH, Nisbet EG, Minshull TA,
812   Lanoisellé M, James RH (2009) Escape of methane gas from the seabed along the West Spitsbergen continental
813   margin. Geophys Res Lett 36
814 Yamanaka T, Mizota C, Fujiwara Y, Chiba H, Hashimoto J, Gamo T, Okudaira T (2003) Sulphur-isotopic
815   composition of the deep-sea mussel Bathymodiolus marisindicus from currently active hydrothermal vents in the
816   Indian Ocean. J. Mar. Biol. Assoc. U. K. 83:841-848
817
818

Figure 1, Prouty et al.

Figure1_Proutyetal

A.

73°50'W   73°40'W

38°10'N

**Baltimore
Canyon**

38°N

5 km

-100

-200

-300

-600

-700

-400

-1200

-1000

-1000

-600

**Baltimore Canyon
Seep Field**

B.

73°51'W   73°50'W   73°49'W

38°4'W

38°3'W

38°2'W

300

400

500

600

2500 m

C.

D.

0

100

200

300

400

500

Depth (m)

0

20

40

60

80

100

Target Strength (dB)

sampled
seep

seafloor

~200 m

Southeast   Northwest

Figure 2, Prouty et al.

Figure2_Proutyetal

A.

74°45'W   74°30'W   74°15'W

5 km

37°N

Norfolk Canyon

Norfolk Seep Field

1800
1700
1600

B.

74°30'W   74°28'W

36°53'N

1500 1400

36°52'N

1600

36°51'N

1700

2 km

C.

sampled seep

D.
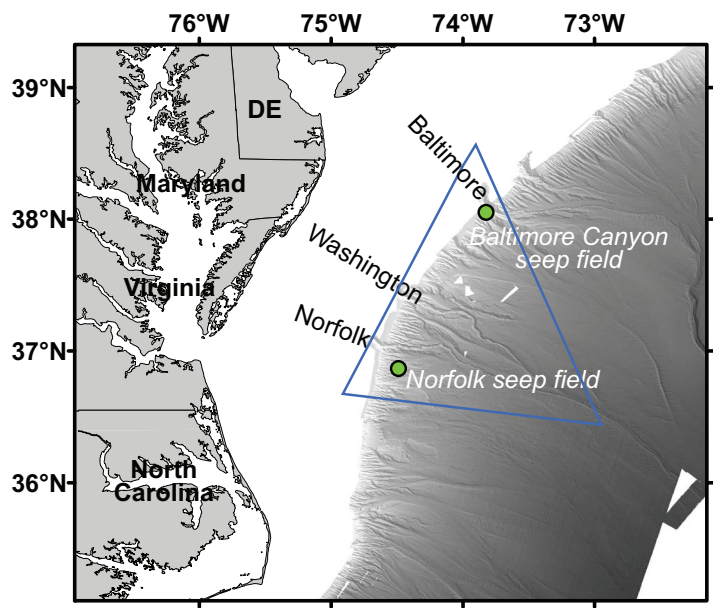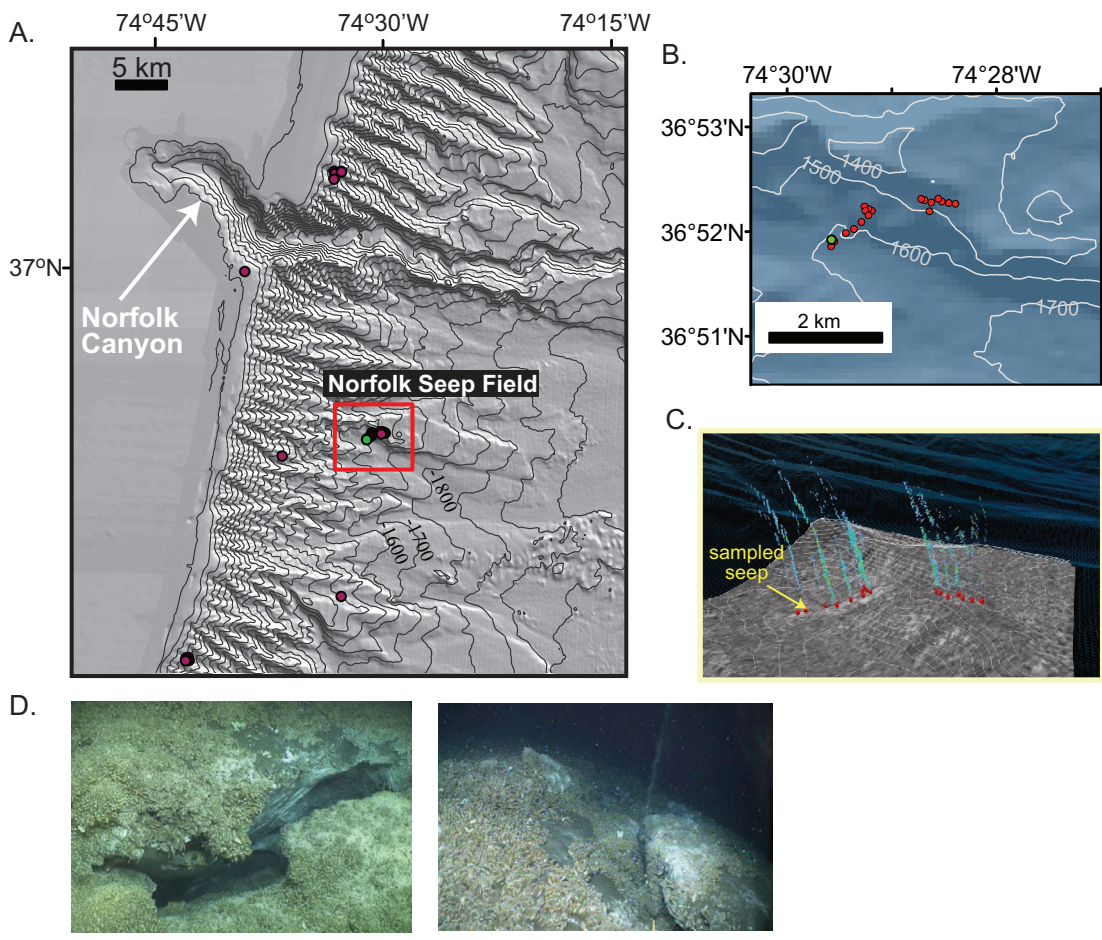
Figure3_prouty et al. Figure 3. Prouty et al.

Norfolk (RB-2013-682)

Baltimore Canyon (NF-2012-14)

Figure4_proutyetal

Figure 5, Prouty et al.
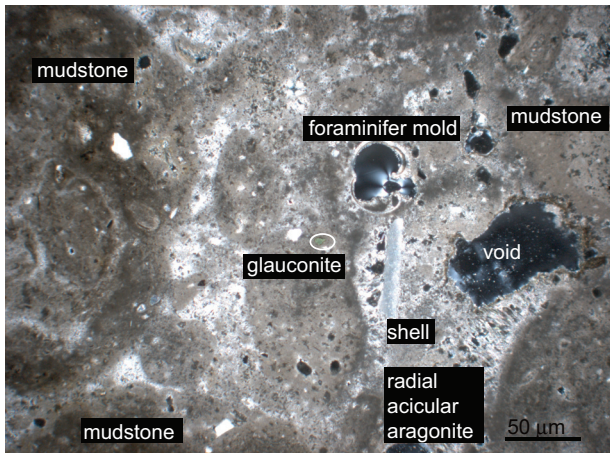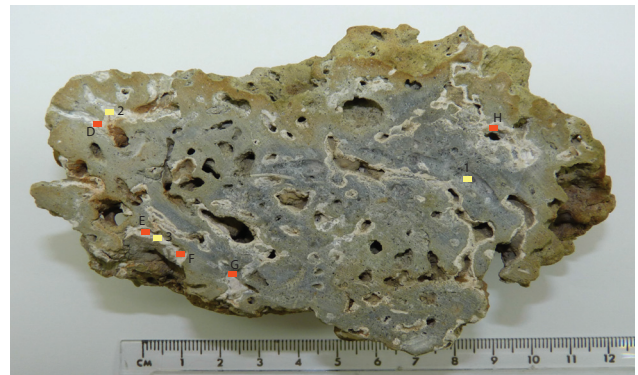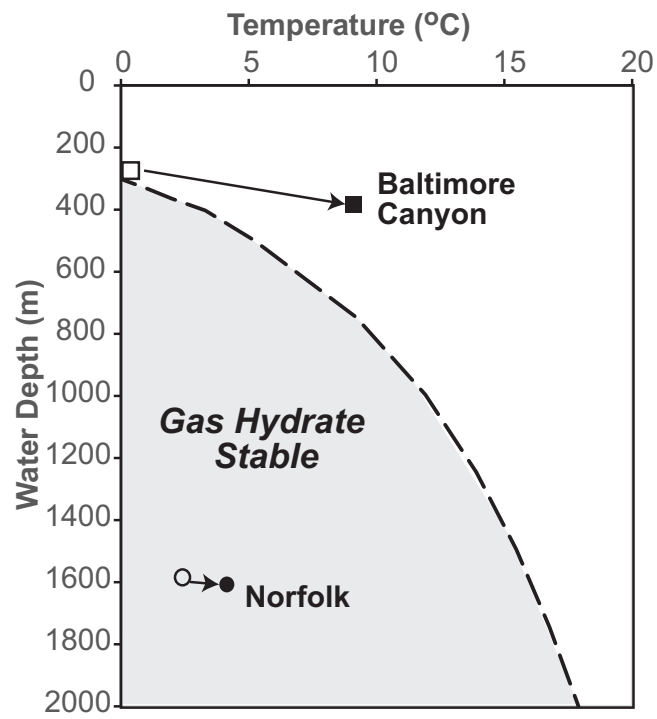
Figure5_proutyetal

Tables

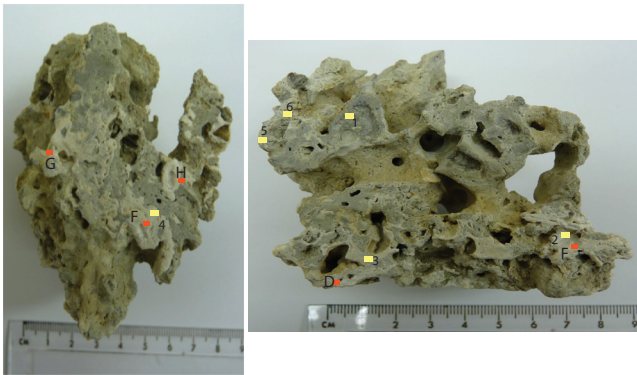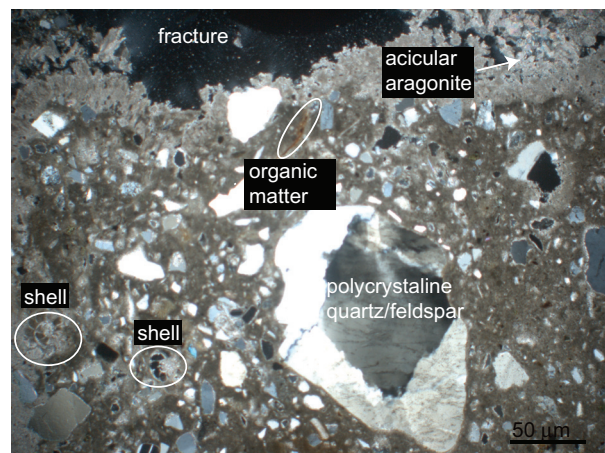|	Sediment		Cement		Groundmass	
	Norfolk	Baltimore Canyon	Norfolk	Baltimore Canyon	Norfolk	Baltimore Canyon
Mineral	-	-	Aragonite	Aragonite	Aragonite	Aragonite
%CaCO$_3$	13.9±6.5	3.3	97.2	85.1	72.5	47.6
%C$_{org}$	3.7±1.4	0.64±0.14	0.16	0.28	0.27	0.39
δ^{13}C (‰)	-31.9±9.0	-23.4±3.0	-47.3±0.16	-49.2±0.21	-44.3±0.07	-47.7±0.92
δ^{18}O (‰)	-	-	3.84±0.07	4.35±0.06	3.78±0.03	3.54±0.04
^{87}Sr/^{86}Sr	-	-	0.70917	0.70918	0.70920	0.70924

Table 1
Mineralogy (dominant carbonate phase), stable isotope, and percent calcium carbonate and organic carbon of authigenic carbonate cement and groundmass and sediment collected at the Norfolk and Baltimore canyons seep sites. Average values reported ±1 standard deviation.

	Mussel Carbonate Shell		Mussel Periostracum	Seawater	
	Norfolk	Baltimore Canyon	Norfolk	Norfolk	Baltimore Canyon
$\delta^{13}C$ (‰)	-2.59±1.68 (-7.10±3.20)	-6.84±1.97	-56.99±12.8	0.90±0.06	-
min	-6.53 (-16.74)	-10.91	-70.66	0.86	
max	0.19 (-3.34)	-3.39	-29.92	0.94	
$\delta^{18}O$ (‰)	3.71±0.25 (3.82±0.39)	2.57±0.28	-	0.34±0.1	0.53±0.1
min	3.11 (3.46)	2.06			
max	4.19 (5.13)	3.59			
$^{87}Sr/^{86}Sr$	0.70920	-	-	0.70917	-
min	0.70918			0.70915	
max	0.70921			0.70920	

Table 2
Geochemical composition of the *Bathymodiolus* sp. shell carbonate and periostracum material and seawater for carbon (±0.04‰), oxygen (±0.06‰), and strontium isotope ratios (±0.00002) for samples collected only at Norfolk. Average and standard deviations are reported. Ranges of values are also reported as minimum and maximum values; values in parenthesis are for dead specimens collected at Norfolk.

	Gill		Periostracum		Sediment	Baltimore Canyon
	Norfolk Seep	Baltimore Canyon	Norfolk Seep	Norfolk Seep	Norfolk Seep	
Average (±σ)	16.58±3.37	14.38±5.15	16.63±4.01	13.89±1.24	5.53±2.16	2.42±3.62
Range	8.65-21.55	-4.07-18.13	8.82-22.65	13.01-14.77	2.98-8.20	-2.62-6.30
n	23	20	28	2	4	5

Table 3
Sulfur isotope (δ^{34}S; ‰) mussel gill and periostracum from *Bathymodiolus* sp. specimens collected at the Norfolk and Baltimore Canyon seep sites and adjacent seep sediment. The average, 1 standard deviation, and ranges of δ^{34}S values are reported.

Station no.	Sample ID	Seep Field Site	Sample type	Fm	±Fm Err	Age	Age Err	Δ¹⁴C (‰)	±Δ¹⁴C Err
RB-13-ROV-682	RB-13-682-1	Norfolk Canyon	authigenic carbonate-groundmass	0.1136	0.0010	17480	80	-887.3	1.0
RB-13-ROV-682	RB-13-682-2	Norfolk Canyon	authigenic carbonate -cement	0.1046	0.0010	18140	80	-896.2	1.0
RB-13-ROV-682	RB-13-682-3	Norfolk Canyon	authigenic carbonate -cement	0.1175	0.0010	17200	80	-883.4	1.0
RB-13-ROV-682	RB-13-682-4	Norfolk Canyon	authigenic carbonate -cement	0.0925	0.0010	19120	90	-908.2	1.0
RB-13-ROV-682	RB-13-682-5	Norfolk Canyon	shell in authigenic carbonate	0.6094	0.0013	3980	20	-395.3	1.3
RB-13-ROV-682	RB-13-682-6	Norfolk Canyon	shell in authigenic carbonate	0.6112	0.0013	3955	20	-393.5	1.3
NF-12-ROV-14	NF-12-14-1	Baltimore Canyon	authigenic carbonate-groundmass	0.0670	0.0010	21710	130	-933.5	1.0
NF-12-ROV-14	NF-12-14-2	Baltimore Canyon	authigenic carbonate -cement	0.0414	0.0010	25570	210	-958.9	1.0
NF-12-ROV-14	NF-12-14-3	Baltimore Canyon	authigenic carbonate -cement	0.2617	0.0011	10770	35	-740.3	1.1
RB-13-ROV-689	RB-13-ROV-689-M6	Baltimore Canyon	mussel shell (alive)	0.8782	0.0017	1045	20	-128.6	1.7
RB-13-ROV-689	RB-13-ROV-689-M6 (rep)	Baltimore Canyon	mussel shell (alive)	0.8747	0.0017	1075	20	-132.0	1.7
RB-13-ROV-689	RB-13-ROV-689-M10	Baltimore Canyon	mussel shell (alive)	0.7859	0.0015	1935	20	-220.2	1.5
RB-13-ROV-687	RB-13-ROV-687	Norfolk Canyon	mussel shell (dead)	0.8114	0.0016	1680	20	-194.9	1.6
RB-13-ROV-687	RB-13-ROV-687 (rep)	Norfolk Canyon	mussel shell (dead)	0.8078	0.0017	1715	20	-198.5	1.7
RB-13-ROV-683	RB-13-ROV-683-Q16A	Norfolk Canyon	mussel shell (dead)	0.7802	0.0015	1995	20	-225.8	1.5
RB-13-ROV-682	RB-13-ROV-682-MQ9	Norfolk Canyon	mussel shell (dead)	0.8558	0.0021	1250	20	-150.8	2.1
RB-13-ROV-682	RB-13-ROV-682- MQ8	Norfolk Canyon	mussel shell (dead)	0.9094	0.0017	765	15	-97.6	1.7
RB-13-ROV-682	RB-13-ROV-682	Norfolk Canyon	mussel shell (dead)	0.8667	0.0018	1150	20	-140.0	1.8
RB-13-ROV-682	RB-13-ROV-682	Norfolk Canyon	mussel shell (dead)	0.8632	0.0021	1180	20	-143.5	2.1
RB-13-ROV-682	RB-13-ROV-682 10% HCl*	Norfolk Canyon	mussel shell (dead)	0.8622	0.0018	1190	20	-144.5	1.8
RB-13-ROV-682	RB-13-ROV-682 10% HCl*	Norfolk Canyon	mussel shell (dead)	0.8624	0.0018	1190	20	-144.2	1.8
RB-13-ROV-683	RB-13-ROV-683-M3	Norfolk Canyon	mussel shell (alive)	0.8937	0.0017	905	20	-113.2	1.7
RB-13-ROV-683	RB-13-ROV-683-M17	Norfolk Canyon	mussel shell (alive)	0.8898	0.0018	940	20	-117.1	1.8
RB-13-ROV-683	RB-13-ROV-683-49	Norfolk Canyon	seawater	0.9837	0.0037	130	30	-23.7	1.7
RB-13-ROV-682	RB-13-ROV-682-2	Norfolk Canyon	seawater	0.9829	0.0027	140	20	-24.6	1.8

Table 4

Summary data results for radiocarbon analysis including ROV station number (Station no.), sample identification (Sample ID), laboratory identification number (Lab ID), seep field, sample type,

fraction modern (Fm) relative to standard, fraction modern error, ¹⁴C age, ¹⁴C age error, Δ¹⁴C value as defined in Stuiver and Polach (1977), and Δ¹⁴C error. Fraction Modern (Fm) is a measurement

of the deviation of the $^{14}C/^{12}C$ ratio of a sample from "Modern." Modern is defined as 95% of the radiocarbon concentration (in AD 1950) of NBS Oxalic Acid I normalized to $\delta^{13}C_{VPDB}$=-19 per mil (Olsson 1970). *Samples pretreated with 10% HCl

				MEASURED				CORRECTED				
Sample Name	Wt (mg)	U (ppm)	232Th (ppb)	$^{230}Th/^{232}Th$ AR(a)	$^{232}Th/^{238}U$ AR(a)	$^{230}Th/^{238}U$ AR(a)	$^{234}U/^{238}U$ AR(a)	$^{230}Th/^{238}U$ AR(b)	$^{234}U/^{238}U$ AR(b)	Rho 08-48	Age (ka)	$^{234}U/^{238}$Ui AR
Carbonate samples												
Norfolk Canyon												
RB-13-682 D	8.8	3.223 ± 0.037	271 ± 3	2.413 ± 0.015	0.02766 ± 0.00002	0.0668 ± 0.0004	1.143 ± 0.001	0.027 ± 0.015	1.146 ± 0.005	0.236	2.6 ± 1.4	1.147 ± 0.006
RB-13-682 E	16.6	3.393 ± 0.021	261 ± 2	2.776 ± 0.012	0.02524 ± 0.00002	0.0701 ± 0.0003	1.143 ± 0.001	0.034 ± 0.013	1.146 ± 0.005	0.238	3.3 ± 1.3	1.147 ± 0.005
RB-13-682 F	12.3	3.427 ± 0.028	65 ± 1	3.844 ± 0.028	0.00623 ± 0.00001	0.0240 ± 0.0002	1.145 ± 0.001	0.015 ± 0.003	1.145 ± 0.002	0.149	1.4 ± 0.3	1.146 ± 0.002
RB-13-682 G	17.2	4.209 ± 0.025	209 ± 1	2.218 ± 0.012	0.01632 ± 0.00001	0.0362 ± 0.0002	1.143 ± 0.001	0.012 ± 0.009	1.145 ± 0.003	0.223	1.2 ± 0.8	1.145 ± 0.003
RB-13-682 H	14.2	3.670± 0.026	160 ± 1	2.231 ± 0.014	0.01435 ± 0.00001	0.0320 ± 0.0002	1.143 ± 0.001	0.011 ± 0.008	1.145 ± 0.003	0.218	1.0 ± 0.7	1.145 ± 0.003
Baltimore Canyon												
NF12-14 D	13.0	3.894 ± 0.030	344 ± 3	5.835 ± 0.017	0.02899 ± 0.00002	0.1692 ± 0.0006	1.139 ± 0.001	0.145 ± 0.009	1.143 ± 0.005	0.301	14.8 ± 1.0	1.149 ± 0.006
NF12-14 E	4.7	4.073 ± 0.087	241 ± 5	8.585 ± 0.036	0.01941 ± 0.00001	0.1667 ± 0.0008	1.140 ± 0.002	0.151 ± 0.006	1.142 ± 0.004	0.283	15.4 ± 0.6	1.148 ± 0.004
NF12-14 F	6.4	4.592 ± 0.072	268 ± 4	8.342 ± 0.029	0.01916 ± 0.00001	0.1598± 0.0006	1.141 ± 0.001	0.144 ± 0.006	1.143 ± 0.004	0.283	14.7 ± 0.6	1.149 ± 0.004
NF12-14 G	4.1	4.588 ± 0.112	433 ± 11	5.682 ± 0.023	0.03103 ± 0.00002	0.1763 ± 0.0008	1.139 ± 0.002	0.151 ± 0.010	1.142 ± 0.006	0.299	15.4 ± 1.0	1.148 ± 0.006
NF12-14 H	6.9	4.110 ± 0.060	586 ± 9	4.087 ± 0.013	0.04681 ± 0.00002	0.1913 ± 0.0007	1.136 ± 0.002	0.153 ± 0.015	1.141 ± 0.009	0.311	15.7 ± 1.6	1.147 ± 0.009
Detritus samples												
Norfolk Canyon												
RB13-D682-PC03 A	77.1	1.959 ± 0.003	8167 ± 14	1.509 ± 0.003	1.36986 ± 0.00113	2.0674 ± 0.0052	0.989 ± 0.001					
RB13-D682-PC03 B	142.9	1.764 ± 0.002	7403 ± 12	1.492 ± 0.003	1.37909 ± 0.00172	2.0576 ± 0.0057	0.989 ± 0.001					
RB13-D682-PC03 C	134.6	1.858 ± 0.002	7865 ± 27	1.467 ± 0.007	1.39116 ± 0.00451	2.0403 ± 0.0089	0.990 ± 0.001					
RB13-D682-PC04 A	75.6	2.165 ± 0.003	7166 ± 12	1.588 ± 0.003	1.08744 ± 0.00082	1.7272 ± 0.0042	1.012 ± 0.001					
RB13-D682-PC04 B	82.1	2.486 ± 0.003	8597 ± 15	1.556 ± 0.004	1.13645 ± 0.00125	1.7682 ± 0.0050	1.008 ± 0.001					
Baltimore Canyon												
NF12-14 1	11.1	2.756 ± 0.025	18081 ± 164	0.680 ± 0.001	2.15602 ± 0.00178	1.4664 ± 0.0037	0.993 ± 0.001					
NF12-14 2	15.0	1.990 ± 0.013	8551 ± 57	0.936 ± 0.002	1.41179 ± 0.00069	1.3208 ± 0.0034	0.995 ± 0.001					
NF12-071-185 B	126.5	1.118 ± 0.001	4119 ± 9	1.118 ± 0.005	1.21060± 0.00220	1.3530 ± 0.0058	1.000 ± 0.001					
NF12-071-185 C	107.6	1.237 ± 0.001	5799 ± 8	0.843 ± 0.002	1.54106 ± 0.00123	1.2984 ± 0.0035	0.994 ± 0.001					

Table 5

Summary data for measured U-Th data for authigenic carbonate samples and activity ratios (AR) used for age calculation and U-Th ages. All activity ratios were calculated using λ^{230}=9.17050E-6, λ^{234}=2.82206E-6 (Cheng et al., 2013), λ^{232}=4.93343E-11 (Holden et al., 1990), λ^{238}=1.55125E-10 (Jaffey et al., 1971), (a) - Activity ratios corrected for hydride formation, tailing, fractionation, SEM-Faraday yield, and tracer isotopic composition, (b) Corrected using average measured detrital U and Th isotopic compositions for the Norfolk Canyon ((^{232}Th/^{238}U) = 1.38, (^{230}Th/^{238}U) = 2.05 and (^{234}U/^{238}U) = 0.99, n=3) and Baltimore Canyon ((^{232}Th/^{238}U) = 1.39, (^{230}Th/^{238}U) = 1.32 and (^{234}U/^{238}U) = 1.00, n=3) sites with all uncertainties arbitrarily set at ± 25% (see main text section 3.5 for details)